Robust Precoding for Massive MIMO LEO Satellite Localization Systems

Yongxiang Zhu, Li You, *Senior Member, IEEE*, Qingfu Kong, Gonzalo Seco-Granados, *Fellow, IEEE*, and Xiqi Gao, *Fellow, IEEE*

***Abstract*—Low earth orbit (LEO) satellite networks combined with massive multiple-input multiple-output (MIMO) technology are expected to support ubiquitous localization with enhanced gains. This paper investigates robust precoding for massive MIMO LEO satellite localization systems under imperfect prior knowledge on user terminals' position. Specifically, we first characterize the signal propagation properties, and derive the squared position error bound (SPEB) to evaluate the localization performance. Then, under imperfect prior position knowledge, we formulate a worst-case sum SPEB minimization problem and propose a codebook-based robust precoding scheme. Simulation results verify the effectiveness of the proposed robust precoding scheme for massive MIMO LEO satellite localization.**

***Index Terms*—LEO satellite, massive MIMO, localization, robust precoding, SPEB.**

I. Introduction

Localization is vital for a range of sixth generation (6G) applications, e.g., location-aware communications, connected automated vehicles, and the Internet of Things. However, the localization performance in a terrestrial network is restricted in some remote areas, where ground infrastructure is infeasible to deploy, or the signals are easily blocked. In these scenarios, satellite networks can effectively complement terrestrial networks by offering larger coverage and supporting more flexible localization [1].

Generally, satellite networks can be classified into geostationary earth orbit (GEO) and non-GEO (NGEO) satellite networks. GEO satellite networks encompass various global navigation satellite systems (GNSSs), including well-known systems like the Global Positioning System (GPS), Galileo, and BeiDou Navigation Satellite System (BDS). Recent advancements have brought extensive attention to low earth orbit (LEO) satellites, particularly in their applications for positioning, navigation, and timing (PNT) [2]. Compared with GEO satellites, LEO satellites can be launched at reduced cost and with increased flexibility [3]. Besides, due to the smaller path loss and larger satellite dynamics, LEO satellite networks demonstrate superior localization capabilities compared with GEO ones [4]. Until now, several LEO satellite communication systems have emerged, including Iridium, Globalstar, OneWeb, Starlink, Telesat, and Hongyun, which can be used as opportunistic systems for positioning, thereby complementing GNSS.

Massive multiple-input multiple-output (MIMO) can provide numerous degrees of freedom in the spatial domain [5]. Besides, it can potentially offer multiple links to perform localization and tracking, and is expected to improve the localization precision [6]. Recently, a 693-square-foot MIMO array has been successfully deployed on Blue Walker 3 LEO satellite by AST SpaceMobile company [7]. Motivated by this, we combine the LEO satellite networks with the employment of massive MIMO, to support localization with the terrestrial user terminals (UTs) in the remote areas.

Despite the precoding designs for localization have been investigated in terrestrial networks [8], [9], the signal propagation characteristics in LEO satellite ones differ significantly, and thus can not be applied directly. Specifically, the larger Doppler shifts and a long propagation delay pose significant challenges in accurately estimating the instantaneous channel state information (iCSI) [10]. Compared with iCSI, statistical CSI (sCSI) is relatively slow-varing and can be obtained with sufficiently high accuracy [11], [12]. Besides, due to the mobility of the UTs or uncertainty in the tracking algorithm, only the coarse knowledge of the UT's position is available at the LEO satellite [13], [14]. Therefore, a robust precoding scheme that takes into account the imperfect prior knowledge on UTs' position is essential to enhance the localization performance.

In this paper, we first derive the squared position error bound (SPEB) as a metric to evaluate the localization performance based on sCSI. Then, we formulate the worst-case sum SPEB minimization problem considering the total power constraint under imperfect prior knowledge. Given the high dimensionality of the problem, we develop an efficient codebook-based scheme to obtain the precoders. Simulation results show the superiority of the proposed scheme.

II. System Model

We consider a massive MIMO LEO satellite localization system consisting of a LEO satellite and K UTs with single-antenna. A uniform planar array (UPA) of $N_{\mathrm{t}} = N_{\mathrm{t}}^{\mathrm{x}} N_{\mathrm{t}}^{\mathrm{y}}$ antennas with half-wavelength separation is applied at the LEO satellite, where $N_{\mathrm{t}}^{\mathrm{x}}$ and $N_{\mathrm{t}}^{\mathrm{y}}$ denote the number of antennas at the x- and y- axes, respectively. The LEO satellite with known position is located at $\mathbf{q} = [q^{\mathrm{x}}, q^{\mathrm{y}}, q^{\mathrm{z}}]^T$ and has an orientation angle of $\boldsymbol{\varphi} = [\varphi_1, \varphi_2]^T$.[1] The unknown position and velocity of the kth UT are denoted by $\mathbf{p}_k = [p_k^{\mathrm{x}}, p_k^{\mathrm{y}}, p_k^{\mathrm{z}}]^T$ and $\dot{\mathbf{p}}_k = [\dot{\mathbf{p}}_k^{\mathrm{x}}, \dot{\mathbf{p}}_k^{\mathrm{y}}, \dot{\mathbf{p}}_k^{\mathrm{z}}]^T$, respectively.[2] We assume fixed positions and velocities of the UTs over the observed interval and update them according to the large movements of the UTs. The system is operated at carrier frequency f_{c} and employs the orthogonal frequency division multiplex (OFDM) modulation with bandwidth B_{w} and sampling period $T_{\mathrm{s}} = 1/2B_{\mathrm{w}}$. Let N_{cp} and N_{sc} denote the number of the cyclic prefix and subcarriers, respectively. The frequency of the nth subcarrier is defined as $f_n = (n - \frac{N_{\mathrm{sc}}+1}{2}) f_{\mathrm{s}}, n = 1, \ldots, N_{\mathrm{sc}}$, where f_{s} is the subcarrier

Received 21 December 2023; revised 23 May 2024; accepted 19 September 2024. Date of publication 26 September 2024; date of current version 14 February 2025. This work was supported in part by the National Natural Science Foundation of China for Outstanding Young Scholars under Grant 62322104, in part by the Key Technologies R&D Program of Jiangsu (Prospective and Key Technologies for Industry) under Grant BE2022067 and Grant BE2022067-5, in part by the Natural Science Foundation of Jiangsu Province under Grant BK20231415, and in part by the Fundamental Research Funds for the Central Universities under Grant 2242022k60007. The work of Gonzalo Seco-Granados was supported in part by the ICREA Academia Program and in part by Spanish R+D Grant PID2023-152820OB-I00. The review of this article was coordinated by Dr. Tomaso De Cola. *(Corresponding author: Li You.)*

Yongxiang Zhu, Li You, Qingfu Kong, and Xiqi Gao are with National Mobile Communications Research Laboratory, Southeast University, Nanjing 210096, China, and also with Purple Mountain Laboratories, Nanjing 211100, China (e-mail: zhuyx@seu.edu.cn; lyou@seu.edu.cn; qfkong@seu.edu.cn; xqgao@seu.edu.cn).

Gonzalo Seco-Granados is with the Department of Telecommunications and Systems Engineering, Universitat Autónoma de Barcelona, 08193 Barcelona, Spain (e-mail: gonzalo.seco@uab.cat).

Digital Object Identifier 10.1109/TVT.2024.3468436

[1] The orientation angle can be obtained and pre-compensated using techniques such as programmed tracking, which considers the predicted movement of the LEO satellite.

[2] We assume the velocity of each UT is known locally by an accelerometer.

seperation. Subsequently, the OFDM symbol length can be given as $T = (N_{\rm cp} + N_{\rm sc})T_{\rm s}$. Specifically, we assume each frame is comprised of $M_{\rm s}$ slots, and there are $M_{\rm sp}$ OFDM symbols for pilot. Consequently, in each frame, a total of $M_{\rm p} = M_{\rm sp}M_{\rm s}$ OFDM symbols are utilized for pilot transmission.

A. Channel Model

In the wideband massive MIMO LEO satellite localization systems, the UPA response $\mathbf{v}_{k,\ell}(f_n)$ for the ℓth propagation path of the kth UT over subcarrier n can be written as

$$\mathbf{v}_{k,\ell}\left(f_n\right) = \mathbf{v}_{\rm x}\left(f_n, \boldsymbol{\theta}_{k,\ell}\right) \otimes \mathbf{v}_{\rm y}\left(f_n, \boldsymbol{\theta}_{k,\ell}\right) \in \mathbb{C}^{N_{\rm t}\times 1}, \tag{1}$$

where $\boldsymbol{\theta}_{k,\ell} = (\theta^{\rm x}_{k,\ell}, \theta^{\rm y}_{k,\ell})$ denotes the angles-of-departure (AoD) pair. In (1), $\mathbf{v}_{\rm x}(f_n, \boldsymbol{\theta}_{k,\ell}) \in \mathbb{C}^{N^{\rm x}_{\rm t}\times 1}$ and $\mathbf{v}_{\rm y}(f_n, \boldsymbol{\theta}_{k,\ell}) \in \mathbb{C}^{N^{\rm y}_{\rm t}\times 1}$ denote the UPA responses of the x- and y-axes, which are defined as [11]

$$\mathbf{v}_{\rm x}\left(f_n, \boldsymbol{\theta}_{k,\ell}\right) = \frac{1}{N^{\rm x}_{\rm t}}\Big[1 \ \exp\left\{-\jmath\varpi_n \sin\theta^{\rm y}_{k,\ell}\cos\theta^{\rm x}_{k,\ell}\right\} \cdots \exp\left\{-\jmath\varpi_n\left(N^{\rm x}_{\rm t}-1\right)\sin\theta^{\rm y}_{k,\ell}\cos\theta^{\rm x}_{k,\ell}\right\}\Big]^T, \tag{2}$$

$$\mathbf{v}_{\rm y}\left(f_n, \boldsymbol{\theta}_{k,\ell}\right) = \frac{1}{N^{\rm y}_{\rm t}}\Big[1 \ \exp\left\{-\jmath\varpi_n \cos\theta^{\rm y}_{k,\ell}\right\} \cdots \exp\left\{-\jmath\varpi_n\left(N^{\rm y}_{\rm t}-1\right)\cos\theta^{\rm y}_{k,\ell}\right\}\Big]^T, \tag{3}$$

where $\varpi_n = \pi(1 + f_n/f_{\rm c})$.

It should be noted that the altitude of the LEO satellite is significantly higher compared to the height of scatterers around the UTs. Therefore, the AoD pair of each propagation path with the kth UT is almost the same [11], [12], i.e., $\boldsymbol{\theta}_{k,\ell} = \boldsymbol{\theta}_k, \forall\ell$,[3] and thus we have $\mathbf{v}_{k,\ell}(f_n) = \mathbf{v}_k(f_n)$. Let $\mathbf{v}_{k,n} = \mathbf{v}_k(f_n)$, and then, with perfect synchronization between the satellite and the UTs in time and frequency,[4] the effective channel vector $\mathbf{h}_{k,m,n} \in \mathbb{C}^{N_{\rm t}\times 1}$ for the kth UT over the nth subcarrier of the mth OFDM symbol is given by [12]

$$\mathbf{h}_{k,m,n} = \mathbf{h}^{\rm los}_{k,m,n} + \mathbf{h}^{\rm nlos}_{k,m,n}, \tag{4}$$

where $\mathbf{h}^{\rm los}_{k,m,n}$ and $\mathbf{h}^{\rm nlos}_{k,m,n}$ represent the line-of-sight (LoS) and non-LoS (NLoS) parts of the channel, respectively, and they can be detailed as $\mathbf{h}^{\rm los}_{k,m,n} = g^{\rm los}_{k,m,n}\mathbf{v}_{k,n}$, $\mathbf{h}^{\rm los}_{k,m,n} = g^{\rm nlos}_{k,m,n}\mathbf{v}_{k,n}$. Let $g_{k,m,n} = g^{\rm los}_{k,m,n} + g^{\rm nlos}_{k,m,n}$, and then, given that there are numerous propagation paths, $g_{k,m,n}$ can be approximated as the aggregate of a great number of independent and identically distributed components, which follows the Rician distribution characterized by average power of $\gamma_k = \mathbb{E}\{|g_{k,m,n}|^2\}$ and a Rician factor of κ_k [15]. Moreover, the LoS complex gain $g^{\rm los}_{k,m,n}$ can be expressed as

$$g^{\rm los}_{k,m,n} = \alpha_k \exp\left\{\jmath 2\pi\left(\nu_k mT - f_n\tau_k\right)\right\}, \tag{5}$$

where ν_k and τ_k are Doppler shifts and propagation delay of the LoS path with UT k, respectively.[5] It is noteworthy that $\alpha_k = \sqrt{\frac{\kappa_k\gamma_k}{1+\kappa_k}}\exp\{\jmath\phi_k\}$, where $\phi_k \in (0, 2\pi]$ represents a random phase. Besides, the NLoS complex gain of the channel follows a distribution as $g^{\rm nlos}_{k,m,n} \sim \mathcal{CN}(0, \gamma_k/(1+\kappa_k))$.

B. System Geometry

The AoD pair of the LoS path of the kth UT, i.e., $(\theta^{\rm x}_k, \theta^{\rm y}_k)$, can be written as [17]

$$\theta^{\rm x}_k = \arctan\left(\frac{p^{\rm r,z}_k}{p^{\rm r,x}_k}\right), \theta^{\rm y}_k = \arccos\left(\frac{p^{\rm r,y}_k}{||\mathbf{p}^{\rm r}_k||_2}\right), \tag{6}$$

where $\mathbf{p}^{\rm r}_k \triangleq \mathbf{R}(\boldsymbol{\varphi})^{-1}(\mathbf{p}_k - \mathbf{q}) \triangleq [p^{\rm r,x}_k, p^{\rm r,y}_k, p^{\rm r,z}_k]^T$ represents the rotated position for the kth UT [18], and $\mathbf{R}(\boldsymbol{\varphi})$ is the rotation matrix [17].

In addition, the Doppler shifts and propagation delay with the LoS path of the kth UT are expressed as [19]

$$\nu_k = -\frac{f_{\rm c}}{c}\frac{\dot{\mathbf{p}}^T_k(\mathbf{p}_k - \mathbf{q})}{||\mathbf{p}_k - \mathbf{q}||_2}, \tau_k = \frac{||\mathbf{p}_k - \mathbf{q}||_2}{c}. \tag{7}$$

C. Performance Metric

The received pilot signal at UT k can be written as

$$y_{k,m,n} = \left(\mathbf{h}^{\rm los}_{k,m,n}\right)^T\mathbf{B}_n\mathbf{s}_{m,n} + \left(\mathbf{h}^{\rm nlos}_{k,m,n}\right)^T\mathbf{B}_n\mathbf{s}_{m,n} + z_{k,m,n}. \tag{8}$$

In (8), $\mathbf{B}_n = [\mathbf{b}_{n,1}, \ldots, \mathbf{b}_{n,K}]$ denotes the precoding matrix, where $\mathbf{b}_{n,k}$ is the precoding vector for UT k. $\mathbf{s}_{m,n} \sim \mathcal{CN}(0, \mathbf{I}_K)$ is the transmitted pilot vector over the nth subcarrier of the mth OFDM symbol, and $z_{k,m,n} \sim \mathcal{CN}(0, N_0)$.

The channel parameters between the LEO satellite and the kth UT are presented as $\boldsymbol{\eta}_k = [\theta^{\rm x}_k, \theta^{\rm y}_k, \tau_k, \nu_k, \alpha^{\rm R}_k, \alpha^{\rm I}_k]^T \in \mathbb{R}^{6\times 1}$, where $\alpha^{\rm R}_k$ and $\alpha^{\rm I}_k$ represent the real and imaginary parts of α_k, respectively. The Fisher information matrix (FIM) for the kth UT can be computed from [20]

$$[\mathbf{J}_{\boldsymbol{\eta}_k}]_{i,j} = \sum_{m=1}^{M_{\rm p}}\sum_{n=1}^{N_{\rm sc}}\frac{2}{N^{\rm eq}_{k,n}}\Re\left\{\mathbb{E}\left\{\frac{\partial\left(r_{k,m,n}\right)^H}{\partial[\boldsymbol{\eta}_k]_i}\frac{\partial\left(r_{k,m,n}\right)}{\partial[\boldsymbol{\eta}_k]_j}\right\}\right\}, \tag{9}$$

where

$$r_{k,m,n} = \left(\mathbf{h}^{\rm los}_{k,m,n}\right)^T\mathbf{B}_n\mathbf{s}_{m,n}, \tag{10}$$

$$N^{\rm eq}_{k,n} = \mathbb{E}\left\{\left|\left(\mathbf{h}^{\rm nlos}_{k,m,n}\right)^T\mathbf{B}_n\mathbf{s}_{m,n} + z_{k,m,n}\right|^2\right\} = \frac{\gamma_k}{1+\kappa_k}\mathbf{v}^T_{k,n}\mathbf{B}_n\mathbf{B}^H_n\mathbf{v}^*_{k,n} + N_0. \tag{11}$$

Note that the required sCSI knowledge involves the channel gain γ_k and the AoD pair $(\theta^{\rm x}_k, \theta^{\rm y}_k)$, which are regarded to be constant during the observed interval and can be updated dynamically in accordance with the channel variation [11]. The position domain unknown parameters are given by $\bar{\boldsymbol{\eta}}_k = [\mathbf{p}^T_k, \alpha^{\rm R}_k, \alpha^{\rm I}_k]^T \in \mathbb{R}^{5\times 1}$. It is worth noting that the transformation from channel parameters $\boldsymbol{\eta}_k$ to position parameters $\bar{\boldsymbol{\eta}}_k$ is a bijection. Then, we derive the FIM $\mathbf{J}_{\bar{\boldsymbol{\eta}}_k}$ of $\bar{\boldsymbol{\eta}}_k$ as

$$\mathbf{J}_{\bar{\boldsymbol{\eta}}_k} = \boldsymbol{\Gamma}_k\mathbf{J}_{\boldsymbol{\eta}_k}\boldsymbol{\Gamma}^T_k. \tag{12}$$

The transformation matrix $\boldsymbol{\Gamma}_k \in \mathbb{R}^{5\times 6}$ can be expressed as

$$\boldsymbol{\Gamma}_k \triangleq \frac{\partial\boldsymbol{\eta}^T_k}{\partial\bar{\boldsymbol{\eta}}_k} = \text{blkdiag}\left\{\boldsymbol{\Xi}_k, \mathbf{I}_2\right\}. \tag{13}$$

The components of $\boldsymbol{\Xi}_k$ are detailed as

$$\boldsymbol{\Xi}_k = \begin{bmatrix}\frac{\partial\theta^{\rm x}_k}{\partial\mathbf{p}_k} & \frac{\partial\theta^{\rm y}_k}{\partial\mathbf{p}_k} & \frac{\partial\tau_k}{\partial\mathbf{p}_k} & \frac{\partial\nu_k}{\partial\mathbf{p}_k}\end{bmatrix} \in \mathbb{R}^{3\times 4}. \tag{14}$$

[3]For an orbit height of about 200 km, the AoD difference of the x- and y-axes are about 0.03° and 0.01° when the scatterers are spread at a maximum radius of 100 m, which can be negligible.

[4]The clock bias/synchronization errors of the different UTs are not incorporated into the models and algorithms of this work. Specifically, synchronization can be assumed to be realized by a tracking algorithm. Besides, in this work, we assume perfect carrier frequency offset synchronization between the UTs and the satellite, which can be obtained and then compensated by under-sampling approach.

[5]The Doppler shift related to the mobility of the LEO satellite can be precompensated due to its deterministic time variation [16].

To quantify the accuracy of position estimation, the sum SPEB of the UTs is adopted as the performance metric, which is given as

$$\rho_{\text{sum}}^{\text{b}}\left(\mathbf{B}_n\right)=\sum_{k=1}^{K}\text{Tr}\left\{\mathbf{E}^T\mathbf{J}_{\bar{\boldsymbol{\eta}}_k}^{-1}\mathbf{E}\right\}, \tag{15}$$

where $\mathbf{E}=[\mathbf{e}_1,\mathbf{e}_2,\mathbf{e}_3]$, and $\mathbf{e}_i\in\mathbb{R}^{5\times1}$ denote a vector with the ith element being one while the others being zero.

III. Precoding Design

The SPEB depends on the parameters in $\bar{\boldsymbol{\eta}}_k$. In this section, we first assume perfect prior knowledge of $\bar{\boldsymbol{\eta}}_k$ and formulate the optimization problem. Then, we will focus on robust precoding with prior uncertainties in $\bar{\boldsymbol{\eta}}_k$.

A. Precoding With Perfect Prior Knowledge

The sum SPEB minimization problem with perfect prior knowledge of $\bar{\boldsymbol{\eta}}_k$ can be formulated as

$$\mathcal{Q}_1:\min_{\mathbf{B}_n}\ \rho_{\text{sum}}^{\text{b}}\left(\mathbf{B}_n\right)\quad\text{s.t.}\ \sum_{n=1}^{N_{\text{sc}}}||\mathbf{B}_n||_F^2\le P, \tag{16}$$

where P is the transmission power budget. Let $\mathbf{X}_n=\mathbf{B}_n\mathbf{B}_n^H$ and problem $\mathcal{Q}_1$ can be converted into a rank-constrained problem

$$\mathcal{Q}_2:\min_{\mathbf{X}_n}\quad\rho_{\text{sum}}^{\text{b}}\left(\mathbf{X}_n\right) \tag{17a}$$

$$\text{s.t.}\quad\sum_{n=1}^{N_{\text{sc}}}\text{Tr}\left\{\mathbf{X}_n\right\}\le P,\mathbf{X}_n\succeq\mathbf{0},\text{rank}\left\{\mathbf{X}_n\right\}\le K. \tag{17b}$$

We introduce an auxiliary variable $\mathbf{M}_k\in\mathbb{R}^{3\times3}$, which satisfies $\mathbf{M}_k\succeq\mathbf{E}^T\mathbf{J}_{\bar{\boldsymbol{\eta}}_k}^{-1}\mathbf{E},\forall k$. By utilizing the property of Schur complement, problem $\mathcal{Q}_2$ can be converted into

$$\mathcal{Q}_3:\min_{\mathbf{X}_n,\mathbf{M}_k}\ \sum_{k=1}^{K}\text{Tr}\left\{\mathbf{M}_k\right\} \tag{18a}$$

$$\text{s.t.}\quad\text{(17b)}, \tag{18b}$$

$$\begin{bmatrix}\mathbf{M}_k & \mathbf{E}^T\\ \mathbf{E} & \mathbf{J}_{\bar{\boldsymbol{\eta}}_k}\left(\mathbf{X}_n\right)\end{bmatrix}\succeq\mathbf{0}. \tag{18c}$$

Note that problem $\mathcal{Q}_3$ has been investigated in the terrestrial systems, where $\mathbf{J}_{\bar{\boldsymbol{\eta}}_k}(\mathbf{X}_n)$ is linearly dependent on $\mathbf{X}_n$. However, for the LEO satellite scenarios, the linear dependence no longer exists, and problem $\mathcal{Q}_3$ requires transformation into a convex problem to be effectively addressed. Therefore, the majorization-minimization (MM) algorithm is invoked to transform $\mathcal{Q}_3$ into a series of convex semidefinite programs (SDPs), the basic philosophy of which is to iteratively handle the problem through a series of easier problems [21]. In Section III-B, we will investigate the robust precoding that takes into account the uncertainties in $\bar{\boldsymbol{\eta}}_k$.

B. Robust Precoding With Imperfect Prior Knowledge

In this part, we assume $\bar{\boldsymbol{\eta}}_k$ belongs to an uncertainty region $\mathcal{U}_k$. The center and the extent of the uncertainty region $\mathcal{U}_k$ can be determined by the means and covariances of the parameters from the output of initial access or tracking [22].

1) Problem Formulation: Under imperfect prior knowledge of $\bar{\boldsymbol{\eta}}_k$, the worst-case sum SPEB minimization strategy is employed for robust precoding design

$$\mathcal{Q}_4:\min_{\mathbf{X}_n}\max_{\bar{\boldsymbol{\eta}}_k\in\mathcal{U}_k}\quad\rho_{\text{sum}}^{\text{b}}\left(\mathbf{X}_n;\bar{\boldsymbol{\eta}}_k\right) \tag{19a}$$

$$\text{s.t.}\quad\text{(17b)}, \tag{19b}$$

By discretizing the uncertainty region $\mathcal{U}_k$ into a uniform grid of G points $\{\bar{\boldsymbol{\eta}}_{k,g}\}_{g=0}^{G-1}$, we introduce auxiliary variables $\{r_k\}_{\forall k}$ to reformulate the problem $\mathcal{Q}_4$ in the epigraph form as [14]

$$\mathcal{Q}_5:\min_{\mathbf{X}_n,r_k,\mathbf{M}_{k,g}}\ \sum_{k=1}^{K}r_k \tag{20a}$$

$$\text{s.t.}\quad\text{(17b)}, \tag{20b}$$

$$\begin{bmatrix}\mathbf{M}_{k,g} & \mathbf{E}^T\\ \mathbf{E} & \mathbf{J}_{\bar{\boldsymbol{\eta}}_{k,g}}\left(\mathbf{X}_n\right)\end{bmatrix}\succeq\mathbf{0},\forall g, \tag{20c}$$

$$\text{Tr}\left\{\mathbf{M}_{k,g}\right\}\le r_k,\forall g, \tag{20d}$$

where $\mathbf{J}_{\bar{\boldsymbol{\eta}}_{k,g}}$ denotes the FIM in (9) evaluated at $\bar{\boldsymbol{\eta}}_k=\bar{\boldsymbol{\eta}}_{k,g}$.

2) Codebook-Based Robust Precoding: Note that the rank constraint of problem $\mathcal{Q}_5$ presents a non-trivial challenge. Thus, we first handle the problem by relaxing this rank constraint [23]. Owing to the presence of numerous grid points $\{\bar{\boldsymbol{\eta}}_{k,g}\}_{g=0}^{G-1}$, problem $\mathcal{Q}_5$ cannot be simplified into a lower-dimensional form, as in [6]. Inspired by [14, Proposition 1], we adopt a low-complexity codebook-based robust precoding scheme to transform $\mathcal{Q}_5$ into a power allocation problem. Specifically, we employ the following codebook to cover the AoD uncertainty intervals of different UTs

$$\mathbf{F}_n\triangleq\left[\mathbf{F}_n^{\text{sum}}\quad\mathbf{F}_n^{\text{diff}}\right], \tag{21}$$

where $\mathbf{F}_n^{\text{sum}}$ denotes a standard directional beam codebook, $\mathbf{F}_n^{\text{diff}}$ denotes a novel derivative codebook, and the detailed elements are given in Appendix.

With the predefined codebook given in (21), we consider the following beam power allocation problem

$$\mathcal{Q}_6:\min_{\substack{\text{diag}(\boldsymbol{\lambda}_n)\\ r_k,\mathbf{M}_{k,g}}}\ \sum_{k=1}^{K}r_k \tag{22a}$$

$$\text{s.t.}\quad\sum_{n=1}^{N_{\text{sc}}}\text{Tr}\left\{\mathbf{F}_n\text{diag}\left(\boldsymbol{\lambda}_n\right)\mathbf{F}_n^H\right\}\le P, \tag{22b}$$

$$\begin{bmatrix}\mathbf{M}_{k,g} & \mathbf{E}^T\\ \mathbf{E} & \mathbf{J}_{\bar{\boldsymbol{\eta}}_{k,g}}\left(\mathbf{F}_n\text{diag}\left(\boldsymbol{\lambda}_n\right)\mathbf{F}_n^H\right)\end{bmatrix}\succeq\mathbf{0},\forall g, \tag{22c}$$

$$\boldsymbol{\lambda}_n\ge\mathbf{0}, \tag{22d}$$

$$\text{Tr}\left\{\mathbf{M}_{k,g}\right\}\le r_k,\forall g, \tag{22e}$$

where $\boldsymbol{\lambda}_n=[\lambda_{n,0}\ \cdots\ \lambda_{n,M-1}]^T$ and $M=3KN_g^xN_g^y$. Note that $\mathbf{J}_{\bar{\boldsymbol{\eta}}_{k,g}}(\mathbf{F}_n\text{diag}(\boldsymbol{\lambda}_n)\mathbf{F}_n^H)$ is not convex concerning the variable $\text{diag}(\boldsymbol{\lambda}_n)$, the MM algorithm is adopted to iteratively handle problem $\mathcal{Q}_6$ through a series of easier problems [21]. Specifically, $\text{diag}(\boldsymbol{\lambda}_{n,t})$ denotes the solution in the tth iteration, and then, we replace $\mathbf{J}_{\bar{\boldsymbol{\eta}}_{k,g}}(\mathbf{F}_n\text{diag}(\boldsymbol{\lambda}_n)\mathbf{F}_n^H)$ by its second order Taylor expansion $\widehat{\mathbf{J}}_{\bar{\boldsymbol{\eta}}_{k,g}}(\mathbf{F}_n\text{diag}(\boldsymbol{\lambda}_n)\mathbf{F}_n^H)$ in $(t+1)$th iteration. The (i,j)th element of $\widehat{\mathbf{J}}_{\bar{\boldsymbol{\eta}}_{k,g}}(\mathbf{F}_n\text{diag}(\boldsymbol{\lambda}_n)\mathbf{F}_n^H)$ is provided in (23), shown at the bottom of the next page, where $\mathbf{C}_{k,m,n,i,j}=\mathbf{F}_n^H\frac{\partial\mathbf{h}_{k,m,n}^*}{\partial[\boldsymbol{\eta}_k]_i}\frac{\partial\mathbf{h}_{k,m,n}^T}{\partial[\boldsymbol{\eta}_k]_j}\mathbf{F}_n$, $\mathbf{Z}_{k,n}=$

$\frac{\gamma_k}{1+\kappa_k}\mathbf{F}_n^H\mathbf{v}_{k,n}^*\mathbf{v}_{k,n}^T\mathbf{F}_n$, and L is the Lipschitz constant [21]. Then, in the $(t+1)$th iteration, the corresponding problem is written as

$$\mathcal{Q}_6^{(t+1)}: \min_{\substack{\text{diag}(\boldsymbol{\lambda}_{n,t+1}) \\ r_{k,t+1},\mathbf{M}_{k,g,t+1}}} \sum_{k=1}^{K} r_{k,t+1} \tag{24a}$$

$$\text{s.t.} \quad \sum_{n=1}^{N_{\text{sc}}} \text{Tr}\left\{\mathbf{F}_n \text{diag}\left(\boldsymbol{\lambda}_{n,t+1}\right)\mathbf{F}_n^H\right\} \le P, \tag{24b}$$

$$\begin{bmatrix} \mathbf{M}_{k,g} & \mathbf{E}^T \\ \mathbf{E} & \widehat{\mathbf{J}}_{\bar{\boldsymbol{\eta}}_{k,g}}\left(\mathbf{F}_n \text{diag}\left(\boldsymbol{\lambda}_{n,t+1}\right)\mathbf{F}_n^H\right) \end{bmatrix} \succeq \mathbf{0}, \forall g, \tag{24c}$$

$$\boldsymbol{\lambda}_{n,t} \ge \mathbf{0}, \tag{24d}$$

$$\text{Tr}\left\{\mathbf{M}_{k,g,t+1}\right\} \le r_{k,t+1}, \forall g. \tag{24e}$$

Note that $\widehat{\mathbf{J}}_{\bar{\boldsymbol{\eta}}_{k,g}}(\mathbf{F}_n \text{diag}(\boldsymbol{\lambda}_n)\mathbf{F}_n^H)$ is convex with resepect to $\text{diag}(\boldsymbol{\lambda}_n)$, and thus can be addressed with SDP solvers [14]. According to [21], the sequence of feasible points $\{\text{diag}(\boldsymbol{\lambda}_{n,t})\}$ can converge to a stationary value. Then, with the nonnegative diagonal matrix $\text{diag}(\boldsymbol{\lambda}_n)$ from $\mathcal{Q}_6$, we have the optimized codebook $\mathbf{F}_n^{\text{opt}} = [\sqrt{\lambda_{n,0}}\mathbf{f}_{n,0} \ \cdots \ \sqrt{\lambda_{n,M-1}}\mathbf{f}_{n,M-1}]$. Then, $\mathbf{B}_n$ can be recovered from $\mathbf{F}_n^{\text{opt}}(\mathbf{F}_n^{\text{opt}})^H$ through Cholesky decomposition and Gaussian randomization approaches. The number of the optimized variables in problem $\mathcal{Q}_6$ is denoted by $n_{\text{var}} = MN_{\text{sc}} + 9KG + 1$. The number of linear matrix inequality (LMI) constraints is $M_{\text{LMI}} = 2KG + N_{\text{sc}}$. Besides, the dimensions of the matrix corresponding to the τth LMI constraint are given by $q_\tau = 3, 1 \le \tau \le KG, q_\tau = 8, KG+1 \le \tau \le 2KG$, and $q_\tau = M_{\text{t}}, 2KG+1 \le \tau \le M_{\text{LMI}}$. By assuming the MM algorithm terminates in J_{mm} iterations, the overall complexity to handle problem $\mathcal{Q}_6$ can be expressed as $\mathcal{O}(J_{\text{mm}} n_{\text{var}}^2 \sum_{\tau=1}^{M_{\text{LMI}}} q_\tau^2 + n_{\text{var}} \sum_{\tau=1}^{M_{\text{LMI}}} q_\tau^3)$ [14].

IV. Simulations

In this section, we evaluate the localization performance for the proposed massive MIMO LEO satellite system. In our simulations, we adopt the average position error band (APEB) to measure the performance of localization, which is defined as $\rho_{\text{avg}}^{\text{b}} = \sqrt{\rho_{\text{sum}}^{\text{b}}/K}$. Some related typical simulation parameters are listed in Table I [6], [14]. The position and the orientation angle of the LEO satellite are assumed to be $\mathbf{q} = [0,0,0]^T$ and $\mathbf{o} = [0,0]^T$, respectively. The AoD pair for the kth UT, i.e., θ_k^{x} and θ_k^{y} are assumed to follow a uniform distribution within the range of $[\pi/3, 2\pi/3]$. The nadir angle of the kth UT can be computed as $\vartheta_k = \arccos(\sin\theta_k^{\text{x}} \sin\theta_k^{\text{y}})$, consequently, the elevation angle of the kth UT is written as $\phi_k = \arccos(\frac{R_{\text{e}}+H}{R_{\text{e}}} \sin\vartheta_k)$, where R_{e} represents the earth radius and H represents the orbit height of the LEO satellite. And the distance between the LEO satellite and the kth UT can be computed as $d_k = \sqrt{H^2 + 2HR_{\text{e}} + R_{\text{e}}^2 \sin^2\phi_k} - R_{\text{e}}\sin\phi_k$. The channel gain γ_k is defined as

$$\gamma_k = G_{\text{sat}} G_{\text{ut}} N_{\text{t}} \left(\frac{c}{4\pi f_c d_k}\right)^2, \tag{25}$$

TABLE I
Simulation Parameters

Parameter	Value
System bandwidth	$B_{\text{w}} = 15.36$ MHz
Carrier frequency	$f_{\text{c}} = 2$ GHz
Subcarrier seperation	$f_{\text{s}} = 30$ KHz
Number of valid subcarriers	$N_{\text{sc}} = 512$
Number of slots per frame	$M_{\text{s}} = 20$
Number of CP	$N_{\text{cp}} = 36$
Rician factor	$\kappa_k = 18$ dB
Number of OFDM symbols per slot	$M_{\text{sp}} = 2$
Orbit height	$H = 200$ km
Antenna spacing	$r_{\text{x}} = r_{\text{y}} = \lambda_c/2$
Antenna gain	$G_{\text{sat}} = 6$ dB, $G_{\text{ut}} = 0$ dB
Number of UTs	$K = 3$
Noise spectral density	-174 dBm/Hz

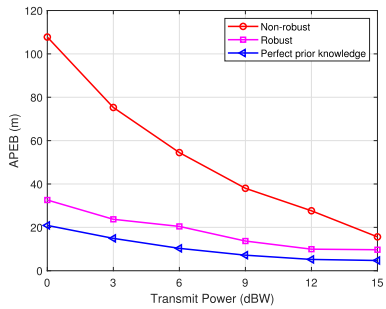

Fig. 1. APEB performance versus transmit power P with $N_{\text{t}} = 576$ antennas.

where G_{sat} and G_{ut} represent the antenna gain at the satellite and the UTs, respectively. The velocity of each UT at x, y, or z-axes is assumed to follow a uniform distribution over the interval $[-10, 10]$ m/s.

Fig. 1 illustrates the relationship between APEB and the transmission power when the number of antennas is set to 576. The robust case presents the APEB value with the proposed worst-case sum SPEB minimization strategy. On the other hand, the non-robust case presents the maximum APEB value in the presence of uncertainties in $\bar{\boldsymbol{\eta}}_k$ employing the strategy in (18). As depicted in Fig. 1, all the curves demonstrate a decreasing trend as the transmission power increases, resulting in enhanced localization performance. Furthermore, by adopting the proposed robust precoding scheme, the robust case APEB performance outperforms the non-robust case under imperfect prior knowledge. It also exhibits APEB performance that closely approaches the performance attained when perfect prior knowledge is available.

Fig. 2 depicts the APEB performance versus the number of antennas when the transmit power is set to 9 dBW. It can be seen that with an increase in the number of antennas, the localization accuracy measured by the APEB is significantly improved in all the cases, which can be

$$\left[\hat{\mathbf{J}}_{\bar{\boldsymbol{\eta}}_{k,g}}\right]_{i,j}\left(\mathbf{F}_n \text{diag}\left(\boldsymbol{\lambda}_n\right)\mathbf{F}_n^H\right) = \left[\mathbf{J}_{\bar{\boldsymbol{\eta}}_{k,g}}\right]_{i,j}\left(\mathbf{F}_n \text{diag}\left(\boldsymbol{\lambda}_{n,t}\right)\mathbf{F}_n^H\right)$$
$$+ \sum_{m=1}^{M}\sum_{n=1}^{N_{\text{sc}}} \text{Tr}\left\{\left(\mathbf{I}_M \odot \frac{\left(\text{Tr}\left\{\mathbf{Z}_{k,n}\text{diag}\left(\boldsymbol{\lambda}_{n,t}\right)\right\} + N_0\right)\mathbf{C}_{k,m,n,i,j} - \text{Tr}\left\{\text{diag}\left(\boldsymbol{\lambda}_{n,t}\right)\mathbf{C}_{k,m,n,i,j}\right\}\mathbf{Z}_{k,n}}{\left(\text{Tr}\left\{\mathbf{Z}_{k,n}\text{diag}\left(\boldsymbol{\lambda}_{n,t}\right)\right\} + N_0\right)^2}\right)^T\right.$$
$$\left. \cdot \left(\text{diag}\left(\boldsymbol{\lambda}_n\right) - \text{diag}\left(\boldsymbol{\lambda}_{n,t}\right)\right)\right\} + \frac{L}{2}||\text{diag}\left(\boldsymbol{\lambda}_n\right) - \text{diag}\left(\boldsymbol{\lambda}_{n,t}\right)||_F^2. \tag{23}$$

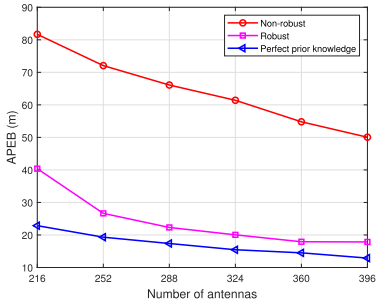

Fig. 2. APEB performance versus antenna numbers N_{t} with $P = 9$ dBW.

attributed to the substantial degrees of freedom offered by the massive number of antennas.

V. Conclusion

To summarize, we investigated robust precoding for massive MIMO LEO satellite localization under imperfect prior knowledge on UTs' position. The performance metric SPEB for localization based on sCSI was derived, based on which we formulated a worst-case sum SPEB minimization problem. To reduce the complexity, we adopted a codebook-based design strategy with the problem transformed into a beam power allocation problem. After that, the MM algorithm was applied to address the non-convexity of this problem. Finally, the solutions were obtained through the SDP solvers. Simulation results indicated that the proposed robust precoding design enhances APEB performance.

Appendix

$\mathbf{F}_n^{\mathrm{sum}}$ and $\mathbf{F}_n^{\mathrm{diff}}$ are defined as $\mathbf{F}_n^{\mathrm{sum}} \triangleq [\mathbf{V}_{1,n} \ \cdots \ \mathbf{V}_{K,n}]$ and $\mathbf{F}_n^{\mathrm{diff}} \triangleq [\mathbf{V}_{1,n,\mathrm{x}} \ \cdots \ \mathbf{V}_{K,n,\mathrm{x}} \ \ \mathbf{V}_{1,n,\mathrm{y}} \ \cdots \ \mathbf{V}_{K,n,\mathrm{y}}]$, where

$$\mathbf{V}_{k,n} \triangleq \left[\mathbf{v}_{k,n,\theta_{k,0}^{\mathrm{x}},\theta_{k,0}^{\mathrm{y}}} \cdots \mathbf{v}_{k,n,\theta_{k,N_g^{\mathrm{x}}-1}^{\mathrm{x}}\ \theta_{k,N_g^{\mathrm{y}}-1}^{\mathrm{y}}}\right], \tag{26}$$

$$\mathbf{V}_{k,n,\mathrm{x}} \triangleq \left[\dot{\mathbf{v}}_{k,n,\dot{\theta}_{k,0}^{\mathrm{x}},\theta_{k,0}^{\mathrm{y}}} \cdots \dot{\mathbf{v}}_{k,n,\dot{\theta}_{k,N_g^{\mathrm{x}}-1}^{\mathrm{x}},\theta_{k,N_g^{\mathrm{y}}-1}^{\mathrm{y}}}\right], \tag{27}$$

$$\mathbf{V}_{k,n,\mathrm{y}} \triangleq \left[\dot{\mathbf{v}}_{k,n,\theta_{k,0}^{\mathrm{x}},\dot{\theta}_{k,0}^{\mathrm{y}}} \cdots \dot{\mathbf{v}}_{k,n,\theta_{k,N_g^{\mathrm{x}}-1}^{\mathrm{x}},\dot{\theta}_{k,N_g^{\mathrm{y}}-1}^{\mathrm{y}}}\right]. \tag{28}$$

Here $\{\theta_{k,i}^{\mathrm{x}}\}_{i=0}^{N_g^{\mathrm{x}}-1}$ and $\{\theta_{k,j}^{\mathrm{y}}\}_{j=0}^{N_g^{\mathrm{y}}-1}$ represent the evenly spaced AoDs that cover the uncertainty interval of the kth UT, with an angular spacing equal to half-power beamwidth [24], and $\dot{\mathbf{v}}_{k,n,\dot{\theta}_{k,0}^{\mathrm{x}},\theta_{k,0}^{\mathrm{y}}} \triangleq \partial \mathbf{v}_{k,n,\theta_{k,0}^{\mathrm{x}},\theta_{k,0}^{\mathrm{y}}} / \partial \theta_{k,0}^{\mathrm{x}}$, $\dot{\mathbf{v}}_{k,n,\theta_{k,0}^{\mathrm{x}},\dot{\theta}_{k,0}^{\mathrm{y}}} \triangleq \partial \mathbf{v}_{k,n,\theta_{k,0}^{\mathrm{x}},\theta_{k,0}^{\mathrm{y}}} / \partial \theta_{k,0}^{\mathrm{y}}$.

References

[1] Z. Gao et al., "Grant-free NOMA-OTFS paradigm: Enabling efficient ubiquitous access for LEO satellite internet-of-things," *IEEE Netw.*, vol. 37, no. 1, pp. 18–26, Apr. 2023.

[2] F. S. Prol et al., "Position, navigation, and timing (PNT) through low earth orbit (LEO) satellites: A survey on current status, challenges, and opportunities," *IEEE Access*, vol. 10, pp. 83971–84002, 2022.

[3] W. Li, Y. Liu, X. Li, and Y. Shen, "Three-dimensional cooperative localization via space-air-ground integrated networks," *China Commun.*, vol. 19, no. 1, pp. 253–263, Jan. 2022.

[4] J. Liu, Y. Shi, Z. M. Fadlullah, and N. Kato, "Space-air-ground integrated network: A survey," *IEEE Commun. Surv. Tuts.*, vol. 20, no. 4, pp. 2714–2741, Fourthquarter 2018.

[5] A. Liu et al., "A survey on fundamental limits of integrated sensing and communication," *IEEE Commun. Surv. Tuts.*, vol. 24, no. 2, pp. 994–1034, Secondquarter 2022.

[6] L. You et al., "Integrated communications and localization for massive MIMO LEO satellite systems," *IEEE Trans. Wireless Commun.*, vol. 23, no. 9, pp. 11061–11075, Sep. 2024.

[7] C. Casetti, "The day 5 G came from outer space [mobile radio]," *IEEE Veh. Technol. Mag.*, vol. 17, no. 4, pp. 5–11, Dec. 2022.

[8] Z. Abu-Shaban, X. Zhou, T. Abhayapala, G. Seco-Granados, and H. Wymeersch, "Error bounds for uplink and downlink 3D localization in 5 G millimeter wave systems," *IEEE Trans. Wireless Commun.*, vol. 17, no. 8, pp. 4939–4954, May 2018.

[9] A. Kakkavas, M. H. C. García, R. A. Stirling-Gallacher, and J. A. Nossek, "Performance limits of single-anchor millimeter-wave positioning," *IEEE Trans. Wireless Commun.*, vol. 18, no. 11, pp. 5196–5210, Aug. 2019.

[10] X. Zhou et al., "Active terminal identification, channel estimation, and signal detection for grant-free NOMA-OTFS in LEO satellite internet-of-things," *IEEE Trans. Wireless Commun.*, vol. 22, no. 4, pp. 2847–2866, Apr. 2023.

[11] L. You, K.-X. Li, J. Wang, X. Gao, X.-G. Xia, and B. Ottersten, "Massive MIMO transmission for LEO satellite communications," *IEEE J. Sel. Areas Commun.*, vol. 38, no. 8, pp. 1851–1865, Aug. 2020.

[12] K.-X. Li et al., "Downlink transmit design for massive MIMO LEO satellite communications," *IEEE Trans. Commun.*, vol. 70, no. 2, pp. 1014–1028, Nov. 2022.

[13] N. Garcia, H. Wymeersch, and D. T. M. Slock, "Optimal precoders for tracking the AoD and AoA of a mmWave path," *IEEE Trans. Signal Process.*, vol. 66, no. 21, pp. 5718–5729, Sep. 2018.

[14] M. F. Keskin, F. Jiang, F. Munier, G. Seco-Granados, and H. Wymeersch, "Optimal spatial signal design for mmWave positioning under imperfect synchronization," *IEEE Trans. Veh. Technol.*, vol. 71, no. 5, pp. 5558–5563, May 2022.

[15] Y. Zhu, P.-Y. Kam, and Y. Xin, "On the mutual information distribution of MIMO Rician fading channels," *IEEE Trans. Commun.*, vol. 57, no. 5, pp. 1453–1462, May 2009.

[16] A. Papathanassiou, A. Salkintzis, and P. Mathiopoulos, "A comparison study of the uplink performance of W-CDMA and OFDM for mobile multimedia communications via LEO satellites," *IEEE Pers. Commun.*, vol. 8, no. 3, pp. 35–43, Jun. 2001.

[17] J. Vince, *Rotation Transforms for Computer Graphics*. London, U.K.: Springer, 2011.

[18] G. Kwon, A. Conti, H. Park, and M. Z. Win, "Joint communication and localization in millimeter wave networks," *IEEE J. Sel. Top. Signal Process.*, vol. 15, no. 6, pp. 1439–1454, Sep. 2021.

[19] Z. Abu-Shaban, G. Seco-Granados, C. R. Benson, and H. Wymeersch, "Performance analysis for autonomous vehicle 5G-assisted positioning in GNSS-challenged environments," in *Proc. IEEE/ION PLANS*, Hilton Portland Downtown, Portland, Apr. 2020, pp. 996–1003.

[20] S. M. Kay, *Fundamentals of Statistical Signal Processing: Estimation Theory*. Englewood Cliffs, NJ, USA: Prentice Hall, 1993.

[21] Y. Sun, P. Babu, and D. P. Palomar, "Majorization-minimization algorithms in signal processing, communications, and machine learning," *IEEE Trans. Signal Process.*, vol. 65, no. 3, pp. 794–816, Aug. 2017.

[22] R. Mendrzik, F. Meyer, G. Bauch, and M. Z. Win, "Enabling situational awareness in millimeter wave massive MIMO systems," *IEEE J. Sel. Top. Signal Process.*, vol. 13, no. 5, pp. 1196–1211, Aug. 2019.

[23] S. Boyd and L. Vandenberghe, *Convex Optimization*. Cambridge, U.K.: Cambridge Univ. Press, 2004.

[24] Y. Yaman and P. Spasojevic, "Beamwidth selection for a uniform planar array (UPA) using RT-ICM mmwave clusters," 2020, *arXiv:2006.05266*.